International Journal of Design & Nature and Ecodynamics
Vol. 21, No. 10, October, 2026, pp. 2835-2846
Journal homepage: http://iieta.org/journals/ijdne

Asymmetric Diurnal Damping of Temperature and Humidity in the Vernacular Leuit Baduy Rice Granary, Indonesia: A Field Diagnostic for Passive Storage Design

Yudi Guntara*, Indri Sari Utami, Yayat Ruhiat

Department of Physics Education, Faculty of Teacher Training and Education, Universitas Sultan Ageng Tirtayasa, Serang 42117, Indonesia

Corresponding Author Email: guntaray@untirta.ac.id

Copyright: ©2026 The authors. This article is published by IIETA and is licensed under the CC BY 4.0 license (http://creativecommons.org/licenses/by/4.0/).

https://doi.org/10.18280/ijdne.211001

Received: 10 August 2026
Revised: 9 October 2026
Accepted: 20 October 2026
Available online: 31 October 2026

Keywords:
amplitude ratio, bio-based materials, hygrothermal damping, Leuit Baduy, post-harvest storage, time lag, vapour pressure, vernacular granary

ABSTRACT

Diurnal swings in temperature (T) and humidity accelerate the post-harvest deterioration of paddy, and mechanically conditioned storage suppresses them at a continuous energy cost. This field diagnostic study examines how the Leuit, a bio-based granary of the indigenous Baduy community in Banten, Indonesia, moderates the microclimate of its paddy stack. Temperature and relative humidity (RH) at the stack centre of three granaries were logged over six to seven diurnal cycles, paired with hourly reanalysis forcing and fitted with a 24 h harmonic model. Damping denotes the reduction of the diurnal amplitude relative to that forcing, irrespective of mechanism. A ratio of logarithmic amplitude damping to phase shift diagnosed diffusion for temperature and was descriptive for RH. At two granaries, the T amplitude ratio was 0.61–0.70 with a 1.3–1.4 h lag, consistent with diffusion within the forcing uncertainty, whereas the RH ratio was 0.20–0.23 with a 2.2–3.0 h lag, which simple diffusion does not reproduce. In-stack vapour pressure peaked within 1 h of in-stack temperature and about 9 h apart from exterior vapour pressure, suggesting a humidity cycle generated locally by temperature-driven sorption. A design translation table and measurement framework turn these preliminary benchmarks into guidance for low-energy tropical storage.

1. INTRODUCTION

Fluctuations in temperature and relative humidity (RH) are a leading cause of post-harvest grain deterioration [1]. Modern storage facilities suppress them through forced convection and mechanical ventilation, which demand a continuous energy input [2]. Vernacular architecture follows the opposite route, in which it moderates the microclimate passively, with local materials and forms adapted to the climate. This principle is now regarded as part of low-carbon design [3, 4]. Envelopes of porous plant biomass therefore deserve study as passive climate moderators, and the knowledge embodied in them as a design resource.

In porous organic media, heat and moisture transfer are coupled. The Luikov system formulates this coupling as an irreversible thermodynamic process in which a temperature gradient drives both conductive heat flux and vapour migration (the Soret effect). Meanwhile, a vapour-pressure gradient drives an additional heat flux (the Dufour effect) [5]. At the pore scale, plant biomass adsorbs water vapour and releases latent heat locally, which causes large temperature variations inside hygroscopic materials [6] and underlies thermochemical energy storage [7]. Models that represent the exchange between free vapour and bound water are now considered necessary to predict the buffering capacity of bio-based materials [8], and sorption hysteresis adds hygric inertia because the adsorption and desorption curves do not coincide [9, 10]. Solving such coupled models requires material properties and boundary data that are rarely available for vernacular structures in use. The present study is therefore empirical and diagnostic, in that it does not perform a Luikov-type assessment. Instead, it uses this framework to pose a question that field data can answer, namely whether the measured response is consistent with simple diffusion or points to an additional mechanism such as sorption.

The amplitude ratio and time lag with which a wall transmits a periodic exterior signal depend on the interplay between material diffusivity and thickness rather than on thermal mass alone [11]. This principle has been applied to vernacular buildings in several regions [12-14]. In addition, indoor–outdoor monitoring of traditional granaries such as the hórreos of northwestern Spain has shown that indoor RH is markedly more stable than outdoor RH, whereas temperature is damped less [15]. Coupled heat–moisture modelling has become standard in building physics [16-18], and that hygroscopic bio-based envelopes damp humidity more strongly and with a longer delay than temperature is also established [8-10, 17, 19, 20]. What remains unreported is a harmonic (amplitude and phase) characterisation of this asymmetry in a humid-tropical granary that stores paddy as panicle bundles and is still in customary use, combined with a diagnostic check of whether one-dimensional diffusion is consistent with it. The claim is restricted to this combination of storage type, stored form and climate.

Studies of Indonesian vernacular architecture have centred on the thermal performance and comfort of dwellings [4, 21, 22], mostly treating humidity as a comfort variable rather than as a transport channel. The literature on the Leuit, the rice granary of the Baduy community in Banten, has developed in the domains of food security, customary law and cultural documentation [23-25], together with ethnoecological accounts of paddy conservation in the Leuit system [26] and a design survey that also recorded microclimate conditions in Baduy Luar Leuit [27]. None of these relates the in-stack response to exterior forcing through amplitude and phase. The gap extends beyond local interest, because unstable storage microclimates recur across the tropics wherever energy infrastructure is limited.

This study therefore pursues three objectives: (i) to measure in situ the amplitude ratio and time lag of the Leuit storage system for temperature and humidity; (ii) to check these parameters against the transient Fourier and Fick solutions through a dimensionless diagnostic ratio that compares logarithmic amplitude damping with phase shift and requires neither wall thickness nor diffusivity; and (iii) to translate the results into provisional design indicators and a measurement framework for low-energy post-harvest storage. Throughout, damping denotes the system-level reduction of the diurnal amplitude at the logged point relative to exterior forcing, irrespective of whether the oscillation is transmitted or generated locally. Figure 1 summarises the resulting two-channel interpretation, namely that the interior temperature behaves as a transmitted, damped exterior wave, whereas the interior vapour pressure appears to be generated locally by sorption in the stored mass.

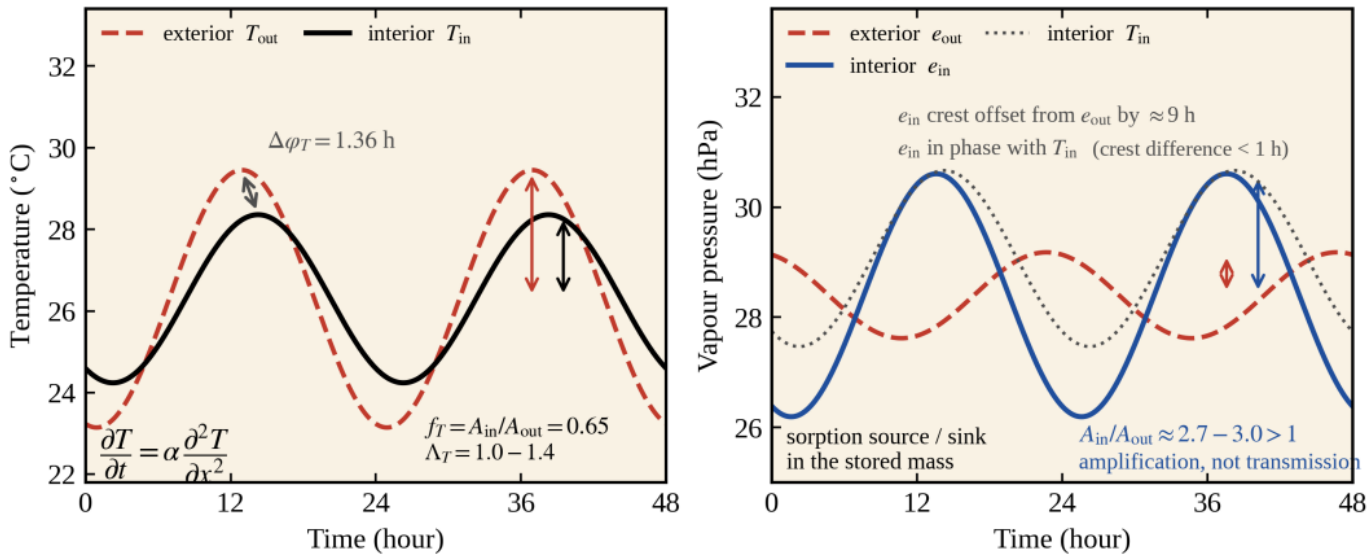

Figure 1. Two-channel framework of hygrothermal transport in the Leuit storage system: (a) thermal channel (transmitted wave) and (b) vapour channel (internal source)
Note: Curves are drawn from the mean harmonic parameters of L1 and L2 (see Section 3).

2. METHODOLOGY

2.1 Study site and specimens

Three Leuit granaries were monitored in the customary territory of the Baduy Luar community, Kanekes Village, Banten Province, Indonesia: Leuit 1 (L1) at 229.7 m above sea level (6°36′35″S, 106°13′18″E), Leuit 2 (L2) at 219.0 m (6°35′32″S, 106°12′41″E) and Leuit 3 (L3) at 285.5 m (6°35′49″S, 106°13′35″E). All three are of the Leuit Lenggang type [24, 26] (Figure 2) and share the same construction: a platform raised above flood-prone ground, a timber frame, walls of tightly woven split bamboo (bilik) clamped by rib boards, a roof of kirai (sago-palm) leaf or sugar-palm fibre, and limited openings for passive cross-ventilation. The storage chamber typically measures about 1.5 m × 1.5 m with a height of up to 4 m and holds roughly 500–600 bundles of paddy [26, 27]. The specimens differ mainly in canopy shading (Section 3.6).

The stored material is ikat padi, bundles of rice panicles still attached to their stalks, which form a stack with a far larger void fraction than loose grain and add straw and husk as lignocellulosic sorption surfaces. Farmers sun-dry the bundles on racks (lantayan) for a few days to more than a week, until grain and stalks are judged dry (owner interviews; see also [26]). Grain moisture at loading was not measured; the practice targets the safe level of at most 14% wet basis set by the national paddy standard [28], used here only as a reference.

Field measurement showed that the bilik panels of the specimens are 0.4–0.5 cm thick, and Section 3.5 uses this value in an order-of-magnitude scale check of the envelope contribution. The diffusivity of the woven bamboo and sugar-palm fibre composite was not determined, which does not affect the diagnostic of Section 2.4 because it depends on neither thickness nor diffusivity.

2.2 Instrumentation and boundary conditions

A Benetech GM1365 digital thermo-hygrometer data logger (manufacturer-stated accuracy ±0.3 °C and ±2.0% RH) was placed in an inter-bundle void at the centre of the paddy stack in each Leuit and recorded at 20 s intervals, giving 4,320 readings per day. The analysis uses hourly means of 180 consecutive readings, which suppress random sensor noise by a factor of about √180. Because the sensor sits inside the stack, the readings describe the storage system as a whole (envelope,

interior air and stored mass) and the interstitial air, not grain moisture content or the room air of the chamber; hereafter, "interior" (subscript in) refers to this in-stack logged point. The loggers were not co-location calibrated. A constant offset between loggers shifts y_0 but leaves A, x_c, f and $\Delta\varphi$ unchanged, because each is computed within one logger's own series; only a span error or a temperature-dependent drift would bias them, and these were not quantified. Baseline values are therefore not compared between specimens.

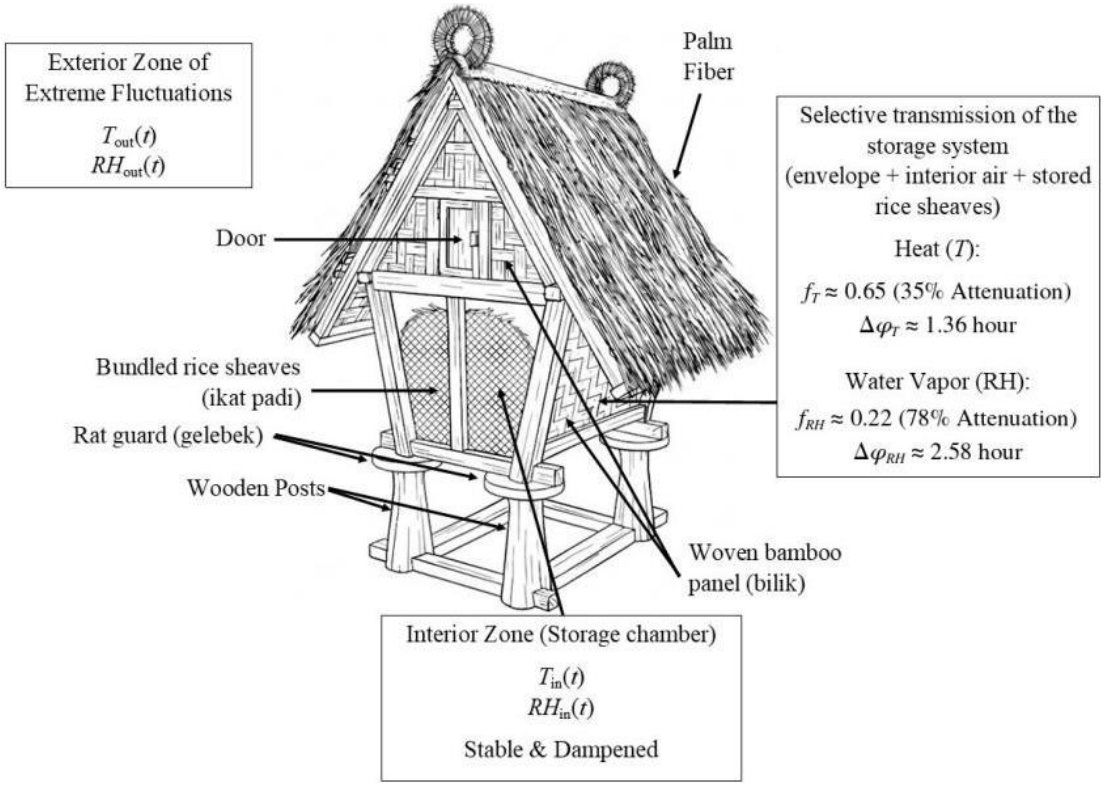

Figure 2. Schematic of the Leuit Lenggang storage system and its hygrothermal zones

The specimens were monitored in separate windows covering whole calendar days: L1 from 9 to 14 September 2024 (144 h, six diurnal cycles), L2 from 29 September to 5 October 2024 (168 h, seven cycles) and L3 from 31 October to 5 November 2024 (144 h, six cycles). Partial records from installation and retrieval days were excluded. The three campaigns span about two months and cross the dry-to-wet season transition in Banten; because the windows did not overlap, specimen effects cannot be separated from those of the weather episode.

Exterior boundary conditions were taken from the hourly NASA POWER database, whose surface parameters derive from the MERRA-2 reanalysis [29]: temperature (T2M), relative humidity (RH2M), dew point (T2MDEW) and specific humidity (QV2M) at 2 m, with corrected precipitation (PRECTOTCORR) used only as seasonal context. Local solar time in the files coincides with Western Indonesia Time at the site, so no shift was needed, and no values were missing. The query points were 6.5957°S/106.2256°E (L1) and 6.5916°S/106.2259°E (L2, L3), with tolerance bands of ±0.5 °C and ±5.0% RH. No ground meteorological station or exterior reference logger was installed, so f and $\Delta\varphi$ characterise the interior response to landscape-scale forcing; they are properties of the system relative to a coarse boundary proxy rather than intrinsic properties of the Leuit, and their sensitivity to forcing error is examined in Section 3.3. Each interior series is paired with its own exterior series, so the per-specimen estimates are internally consistent, but the three specimens cannot be compared as a spatial gradient. The total measurement uncertainty U_{total} combines the internal (logger) and external (satellite) terms by root-sum-square, Eq. (1):

$$U_{\text{total}} = \sqrt{(U_{\text{internal}})^2 + (U_{\text{external}})^2} \quad (1)$$

which gives ±0.58 °C for temperature and ±5.39% for RH.

2.3 Harmonic model and derived variables

The diurnal microclimate fluctuation was modelled as a sinusoid with a 24 h period, Eq. (2):

$$y(t) = y_0 + A\,sin\left[\frac{\pi(t - x_c)}{W}\right] \quad (2)$$

where, $y(t)$ is the measured variable (T or RH) at time t (h), y_0 the baseline mean, A the amplitude, x_c the phase shift and W = 12 h the half period; the crest occurs at $t = x_c + 6$. Fitting used unweighted Levenberg–Marquardt nonlinear least squares on the n hourly means. Parameter standard errors (SE) came from the asymptotic covariance matrix scaled by the residual variance s^2 (residual sum of squares divided by $n - 4$), so that they reflect the observed scatter rather than the sensor specification; because hourly residuals are serially correlated, they remain lower bounds (Appendix A1). The signal-to-noise ratio (SNR) = $|A|/s$ compares each amplitude with the residual standard deviation (SD). The temperature amplitude is positive and the RH amplitude negative in every exterior and interior series of L1 and L2, reflecting the near-antiphase of temperature and humidity in a humid tropical climate (crests 10.6 to 12.3 h apart); $|A|$ will be reported in detail in the

following section. Because interior and exterior signs agree in every pair analysed, the phase difference remains a valid time lag. The amplitude ratio f and the time lag $\Delta\varphi$ follow from Eqs. (3) and (4):

$$f = A_{in}/A_{out} \tag{3}$$

$$\Delta\varphi = x_{c,in} - x_{c,out} \tag{4}$$

Because the exterior amplitude comes from a landscape-scale reanalysis, f is the ratio of the interior amplitude to landscape-scale forcing and not the envelope decrement factor in the strict building-physics sense.

Water-vapour pressure e was derived as a third variable, because RH depends on both vapour content and temperature and is therefore not the driving potential for the Fickian diffusion of Eq. (5b). Interior e was computed at the native 20 s resolution before hourly averaging, since e is a nonlinear function of T and RH and averaging first would introduce bias. Two independent estimators were used: the Magnus equation applied to T and RH, and the dew-point temperature recorded by the logger. Exterior e was derived from QV2M at an atmospheric pressure of 985 hPa and cross-checked against the RH2M–T2M pair and T2MDEW. Fit quality was assessed with the coefficient of determination (R^2), SNR and the SE of each parameter. For interior e, a conservative upper bound on SE(x_c) was obtained by propagating the residual SDs of T and RH through the linearised Magnus relation, assuming fully correlated residuals (Appendix A2).

2.4 Diagnostic check against the transient diffusion solution

To check whether passive diffusion alone is consistent with the damping and lag, the fitted parameters were compared with the analytical solution of one-dimensional transient diffusion in a semi-infinite slab under sinusoidal excitation. Fourier's second law governs the heat channel, Eq. (5a), and Fick's second law governs the water-vapour channel, Eq. (5b):

$$\frac{\partial T}{\partial t} = \alpha \frac{\partial^2 T}{\partial x^2} \tag{5a}$$

$$\frac{\partial P_V}{\partial t} = D_{eff} \frac{\partial^2 P_V}{\partial x^2} \tag{5b}$$

For an effective path length L, the transmitted amplitude decays exponentially with depth while its phase shifts, which yields two identities at the diurnal angular frequency $\omega = \pi/12$ rad h^{-1}, Eqs. (6) and (7):

$$-\ln f = L\sqrt{\frac{\omega}{2\alpha}} \tag{6}$$

$$\omega\Delta\varphi = L\sqrt{\frac{\omega}{2\alpha}} \tag{7}$$

The right-hand sides of Eqs. (6) and (7) are identical, so L and α cancel and the two left-hand sides can be compared directly through the dimensionless diagnostic ratio Λ, Eq. (8):

$$\Lambda = \frac{(-\ln f)}{(\omega\Delta\varphi)} \tag{8}$$

$\Lambda = 1$ when linear, constant-coefficient Fourier–Fick diffusion fully governs the transmission. $\Lambda > 1$ means that the amplitude is damped more strongly than the observed lag can explain, so a mechanism stores amplitude without slowing the wave front proportionately; reversible hygroscopic sorption is the principal candidate [8-10, 17-20]. $\Lambda < 1$ indicates a faster parallel path, such as advection through ventilation openings. Λ thus compares the damping term $-\ln f$ with the phase term $\omega\cdot\Delta\varphi$ of the same variable. It is a mechanistic diagnostic only for T; because RH is not a transported potential and the exterior RH is clipped at saturation, Λ_{RH} is descriptive, and the vapour channel is examined through the phase relations of e (Section 3.4). Because the semi-infinite assumption does not strictly hold for a thin, ventilated wall, Λ is used as a comparative diagnostic within each specimen, not as a formal test. Its sensitivity to errors in the reanalysis forcing was examined by scaling the exterior amplitude by a factor k or shifting the exterior phase by δ, and by finding the k or δ at which $\Lambda = 1$.

2.5 Research ethics and community permission

Fieldwork took place within the customary territory of the Baduy community. Oral consent to observe and instrument the Leuit was obtained from the customary head before fieldwork, following the procedure recognised in Kanekes Village, where the governance of the Leuit is itself subject to customary law [25]. No personal or human-subject data were collected; the measurements were confined to physical environmental variables, and local practices and knowledge are attributed to the Baduy community as their owners.

2.6 Reproducibility note: Data sources and code

The exterior series can be retrieved again from the hourly point API of NASA POWER (https://power.larc.nasa.gov), which serves surface meteorology derived from MERRA-2 [29]. The queries requested T2M (°C), RH2M (%), T2MDEW (°C), QV2M (g kg^{-1}) and PRECTOTCORR (mm d^{-1}) in local solar time for the Sustainable Buildings (SB) user community, at 6.5957°S, 106.2256°E for L1 from 9 to 14 September 2024, and at 6.5916°S, 106.2259°E for L2 from 29 September to 5 October 2024 and for L3 from 31 October to 5 November 2024 (whole days; 144, 168 and 144 h). The Supplementary Material contains the complete raw 20 s logger records, the NASA POWER files as downloaded, the hourly interior and exterior series used in every fit, and three Python 3 scripts with a README file. get_nasa_power.py repeats the queries; leuit_analysis.py computes e at 20 s, forms the hourly means, fits Eq. (2) and generates the summary statistics, the peak-to-peak ranges (Table S1 in Supplementary Material) and corresponding figure; check_derived_tables.py recomputes the derived results from the primary dataset without external data files. After installing the listed packages (pip install-r requirements.txt), running python scripts/leuit_analysis.py in the package folder reproduces the reported values.

3. RESULTS AND DISCUSSION

3.1 Harmonic fit parameters

Table 1 lists the fitted harmonic parameters, with their SE, SNRs and coefficients of determination, for every specimen,

variable and location, and Figure 3 shows the complete time series with the fitted curves. Black symbols denote interior data, red symbols the exterior boundary conditions, error bars the measurement uncertainty and continuous lines Eq. (2). Amplitudes are half-amplitudes; raw peak-to-peak ranges are given in Table S1 in Supplementary Material. The exterior RH series is not fully sinusoidal, because it flattens near saturation at night (20 to 36 h above 95%, with maxima of 96.3 to 97.0%). The harmonic model cannot represent a clipped crest, so the fitted curves exceed 100% for L1 and L2, and the fundamental harmonic of a clipped series misrepresents both its amplitude and its phase. All RH-derived parameters (f_{RH}, $\Delta\varphi_{RH}$ and Λ_{RH}) are therefore treated as descriptive system-level indicators, and mechanistic inference on the moisture channel rests on e (Section 3.4), whose exterior estimate from QV2M is not truncated in the same way.

Table 1. Harmonic fit parameters for the three Leuit specimens

Specimen	Variable	Location	y_0	A (±SE)	x_c (h) (±SE)	R^2	SNR
L1 (229.7 m)	T (°C)	Interior	25.93	1.99 ± 0.11	8.35 ± 0.21	0.701	2.13
L1 (229.7 m)	T (°C)	Exterior	25.92	3.27 ± 0.12	6.96 ± 0.14	0.839	3.19
L1 (229.7 m)	RH (%)	Interior	84.52	3.95 ± 0.34	8.94 ± 0.33	0.496	1.38
L1 (229.7 m)	RH (%)	Exterior	83.30	16.87 ± 0.67	6.78 ± 0.15	0.818	2.96
L2 (219.0 m)	T (°C)	Interior	26.68	2.13 ± 0.11	8.20 ± 0.20	0.698	2.12
L2 (219.0 m)	T (°C)	Exterior	26.91	3.04 ± 0.10	6.87 ± 0.13	0.850	3.33
L2 (219.0 m)	RH (%)	Interior	86.05	3.33 ± 0.22	9.57 ± 0.25	0.591	1.68
L2 (219.0 m)	RH (%)	Exterior	83.57	16.41 ± 0.55	6.57 ± 0.13	0.845	3.26
L3 (285.5 m, shaded)	T (°C)	Interior	26.70	0.29 ± 0.05	11.76 ± 0.70	0.174	0.64
L3 (285.5 m, shaded)	T (°C)	Exterior	26.36	2.77 ± 0.17	6.92 ± 0.23	0.668	1.98
L3 (285.5 m, shaded)	RH (%)	Interior	85.38	0.47 ± 0.11	9.76 ± 0.92	0.110	0.49
L3 (285.5 m, shaded)	RH (%)	Exterior	82.95	15.62 ± 0.69	6.55 ± 0.17	0.787	2.68

Note: Standard errors (SE) are residual-based (Section 2.3); SNR = $|A|/s$, with s the residual standard deviation (SD). R^2: coefficient of determination; SNR: signal-to-noise ratio.

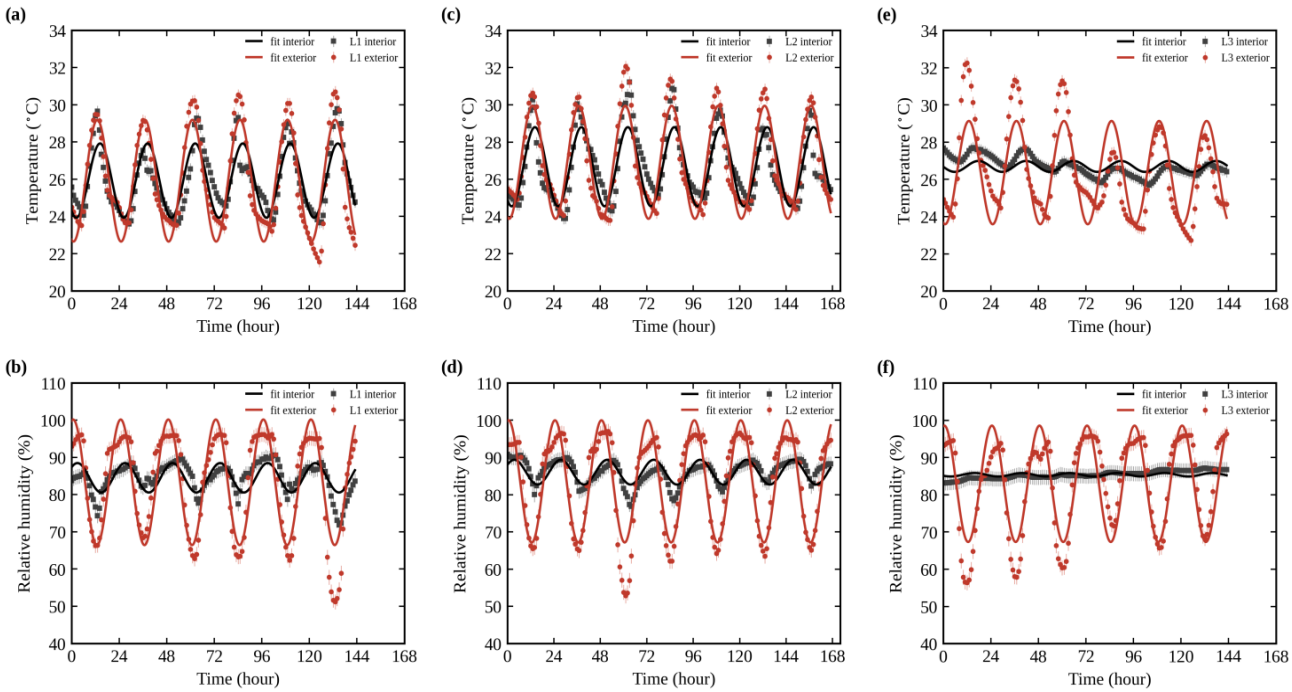

Figure 3. Microclimate time series with the fitted harmonic curves: (a), (c), (e) temperature at L1, L2 and L3; (b), (d), (f) relative humidity (RH) at L1, L2 and L3

3.2 Amplitude ratio and time lag

Table 2 gives f and $\Delta\varphi$ for L1 and L2, the specimens with measurable exterior excitation (L3 is treated in Section 3.6). Averaged over the two, the system reduces the temperature amplitude to about 65% of its exterior value (relative to the reanalysis forcing) with a lag of 1.36 h, and the RH amplitude to about 22% with a much longer lag of 2.58 h. Each specimen reproduces this asymmetry individually, and it is the central empirical observation of this study. With only two independent units, monitored in different weather windows, the spread is descriptive rather than a population confidence interval.

The interior RH fits have markedly lower R^2 (0.496 at L1 and 0.591 at L2) than the exterior fits. Table 1 shows why: their SNR is only 1.38 and 1.68, against 2.96 and 3.26 for the exterior RH, so the residual scatter (s = 2.9% and 2.0% RH) is comparable to the fitted amplitude. That scatter is not sensor noise, which hourly averaging largely removes, but day-to-day drift and departures from a sinusoidal waveform, which saturation and nonlinear sorption make likely. The fundamental harmonic nevertheless remains well determined: the fitted amplitudes lie more than eleven SE from zero and the interior phases have SE of 0.25 to 0.33 h. R^2 is therefore

read as the share of variance carried by the 24 h component, not as evidence for or against the fitted parameters.

Table 2. Amplitude ratio and time lag for the specimens with measured exterior excitation

Specimen	Variable	f (±SE)	$\Delta\varphi$ (h) (±SE)
L1	T	0.609 ± 0.041	1.39 ± 0.25
L1	RH	0.234 ± 0.022	2.16 ± 0.36
L2	T	0.700 ± 0.043	1.33 ± 0.23
L2	RH	0.203 ± 0.015	3.00 ± 0.28
Mean (n = 2)	T	0.655 ± 0.064 (SD)	1.36 ± 0.04 (SD)
Mean (n = 2)	RH	0.218 ± 0.022 (SD)	2.58 ± 0.59 (SD)

Note: SE: standard error, RH: relative humidity, SD: standard deviation.

3.3 Fourier–Fick diagnostic

Table 3 shows that the two channels behave qualitatively differently. For temperature, Λ is 1.36 ± 0.31 at L1 and 1.03 ± 0.25 at L2, both within about one SE of unity (Figure 4(a)). For RH, both specimens yield Λ above unity and in the same direction (2.57 ± 0.46 and 2.03 ± 0.21, i.e., 3.4 and 4.9 SE away). These SEs ignore errors in the forcing itself, and the temperature result is sensitive to them: Λ_T would equal one if the local exterior amplitude were 12% (L1) or 1% (L2) smaller than the reanalysis value, or if the local exterior crest occurred 0.5 h earlier at L1. Λ_T is therefore consistent with diffusion but does not discriminate between mechanisms. For RH, Λ = 1 would require a local exterior amplitude below 41 to 44% of the reanalysis value or an exterior crest 3.1 to 3.4 h earlier; such a bias cannot be excluded without on-site sensors, so $\Lambda_{RH} > 1$ is conditional on the forcing proxy (Table A1). Since RH is not a driving potential and its exterior series is clipped, Λ_{RH} shows only that the interior humidity dynamics do not follow a simple diffusive form; it does not identify the mechanism, which is examined in vapour pressure in Section 3.4.

Table 3. Diagnostic ratio against the transient diffusion solution

Specimen	Variable	$-\ln f$	$\omega\cdot\Delta\varphi$	Λ
L1	T	0.495 ± 0.066	0.363 ± 0.066	1.36 ± 0.31
L2	T	0.357 ± 0.061	0.347 ± 0.061	1.03 ± 0.25
L1	RH	1.451 ± 0.094	0.565 ± 0.094	2.57 ± 0.46
L2	RH	1.596 ± 0.073	0.785 ± 0.073	2.03 ± 0.21
Mean	T	0.426	0.355	1.20
Mean	RH	1.524	0.675	2.30

Note: $\Lambda = (-\ln f)/(\omega\cdot\Delta\varphi)$ with $\omega = \pi/12$ rad h^{-1}; pure Fourier–Fick diffusion gives Λ = 1; SE propagated from the residual-based SE in Table 1.

Table 4. Phase relations bearing on the source of the interior humidity oscillation

Specimen	x_c of T_{in} (h)	x_c of e_{in} (h)	Difference (h)	x_c of e_{out} (h)
L1	8.35 ± 0.21	7.80 (≤0.62)	−0.55 (≤0.66)	16.83
L2	8.20 ± 0.20	7.42 (≤0.40)	−0.78 (≤0.44)	16.59

Note: Values in parentheses are conservative upper bounds on the SE (Section 2.3). The second to fourth columns derive from the interior logger alone; e_{in} is computed from the logger dew point.

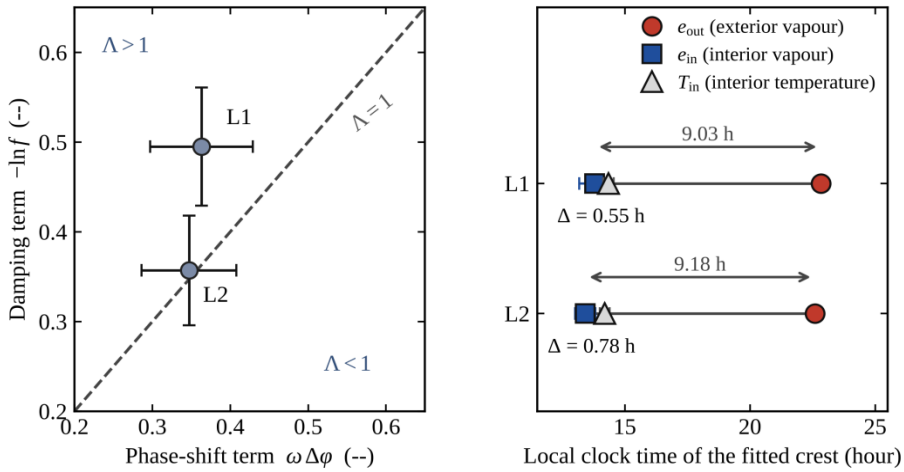

Figure 4. Fourier–Fick diagnostic and vapour-phase relations: (a) damping versus phase-shift terms for the L1 and L2 temperature channel (error bars: residual-based SE; dashed line: Λ = 1); (b) crest times of interior vapour pressure, interior temperature and exterior vapour pressure

3.4 Vapour-pressure channel: Evidence for a locally generated humidity cycle

The most robust evidence comes from the interior logger alone and involves no satellite boundary condition. Table 4 shows that interior vapour pressure is nearly in phase with interior temperature (crest-time differences of 0.55 and 0.78 h, against conservative SE bounds of 0.66 and 0.44 h), whereas its crest is offset by about nine hours from that of exterior vapour pressure (Figure 4(b)). Because the fitted phase of a single harmonic over whole cycles equals the phase of the series at the 24 h frequency, these differences are cross-phase estimates at that frequency; correlation coefficients of the autocorrelated series are not used as evidence. Because the interior e amplitude is positive and the exterior amplitude negative, the raw x_c difference of about three hours is not a valid lag (Section 2.3); expressed as crest times, exterior e peaks at 22.8 and 22.6 h local time and interior e at 13.8 and 13.4 h. If the vapour filling the inter-bundle voids came from outside air penetrating the envelope, interior e would follow exterior e with a short lag and in the same direction; it would not be locked to the interior temperature. At the logged point,

the data show the opposite.

The mechanism consistent with this pattern is temperature-driven sorption and desorption in the hygroscopic mass inside the Leuit. As the interior warms during the day, the sorption equilibrium shifts and the paddy bundles and envelope matrix release water vapour into the interstitial air; as it cools at night, both take it up again. The stored mass and the envelope therefore appear to act as internal vapour sources and sinks rather than merely as diffusion barriers; because advection and sorption were not measured directly, this attribution remains an inference.

Table 5 corroborates this conclusion. The exterior vapour-pressure amplitude is very small (0.61 and 0.95 hPa against means of 27.6 and 29.4 hPa), and three independent derivations from NASA POWER (QV2M, RH2M–T2M and T2MDEW) agree within 0.24 hPa. The interior-to-exterior amplitude ratio is therefore about three for both specimens and both interior estimators. Passive transmission cannot amplify a wave, and Λ cannot be evaluated because $-\ln f$ becomes negative. The nearly flat reanalysis humidity may, however, reflect smoothing over the 56 km × 69 km grid cell; the ratios would be wholly artefactual only if the product underestimated the true amplitude threefold. The small exterior amplitude also makes the exterior e phase less certain than the interior phases. As this cannot be excluded without ground data, Table 5 is treated as corroboration and Table 4 as the foundation.

Table 5. Vapour-pressure amplitudes

Specimen	A Interior (hPa)	A Exterior (hPa)	Amplitude Ratio	Crest Offset (h)
L1	1.82 (2.02)	0.61	2.99 (3.32)	−9.03 (−8.89)
L2	2.60 (2.73)	0.95	2.73 (2.87)	−9.18 (−9.03)

Note: Values outside parentheses use the logger dew point; values inside parentheses use the Magnus equation applied to T and RH (Section 2.3).

This interpretation changes the meaning of the humidity results in Sections 3.2 and 3.3 without invalidating their empirical value. The ratio $f_{RH} = 0.22$ correctly describes the stability of the interior microclimate, which is the sense in which damping is used here (Section 1), but it does not represent the damping of a transmitted humidity wave. The temperature channel is unaffected, because temperature is a genuine transport variable, although Λ_T remains conditional on the forcing proxy (Section 3.3).

3.5 Contributing mechanisms

Because the logger sits inside the stack of paddy bundles, f and $\Delta\varphi$ describe the envelope, interior air and stored mass together. Its sorption reservoir comprises two groups of lignocellulosic material. In the envelope, bamboo shows marked sorption hysteresis [30, 31] and excellent moisture buffering in fibreboard form [32]; sugar-palm fibre is rich in hemicellulose [33], which raises hygroscopicity while lignin suppresses it [34], although its properties as an envelope material have never been measured. In the stored mass, straw and husk offer a large exposed surface: rice straw has well-characterised sorption isotherms [35] and high buffering capacity in composites [36], and the rice caryopsis is itself hygroscopic, with documented hysteresis [37, 38].

The system thus behaves as a packed bed of hygroscopic particles that act as vapour sources and sinks, exchanging with the inter-particle air on their own time constant, distinct from that of the bed [39]. This is consistent with Tables 4 and 5: the interstitial air exchanges vapour with the surrounding mass in step with local temperature, and the large, temperature-sensitive sorption capacity explains why the resulting oscillation can exceed the exterior amplitude. Bio-based materials generally show smaller temperature variation than conventional insulation partly through the same mechanism and its latent heat [6, 40].

The measured bilik thickness permits an order-of-magnitude scale check, not an estimate of wall properties. If the envelope alone produced the response, and the reanalysis forcing acted directly on its outer surface, Eqs. (6) and (7) with $L = 0.45$ cm would imply an effective thermal diffusivity of 3.0×10^{-9} to 6.1×10^{-9} m^2 s^{-1}, about 20–45 times smaller than that of bamboo, which is of order 1.3×10^{-7} m^2 s^{-1} for a conductivity of 0.15 W m^{-1} K^{-1}, a density of 700 kg m^{-3} and a specific heat of 1,600 J kg^{-1} K^{-1}. Equivalently, the observed damping would require a conduction path of 2 to 3 cm of solid bamboo, five to seven times the actual panel thickness. The check also assumes one-dimensional conduction, no surface resistances or radiation, and no storage in the interior air and stored mass, none of which holds for a logger placed in the stack. It therefore shows only that the envelope is unlikely to account for the response on its own and that the stack and interior air contribute; it does not quantify their shares, which would require sensors on the inner wall surface.

Advection through the ventilation openings and the porous stack is a further pathway that the diffusion framework does not represent and that was not measured; humidity Λ values above unity suggest only indirectly that it does not dominate the vapour channel at the diurnal scale.

For storage quality, the interior RH baseline of 84.5 to 86.1% is not low, and storage moulds develop over a range that includes these values [41, 42]. The study therefore quantifies stability, not reduction, of interior humidity: the residual oscillation is a reversible internal sorption exchange rather than an influx of ambient vapour, and its preservation value lies in suppressing the daily wetting-and-drying cycle that can trigger local condensation and microbial hot spots. Initial drying reinforces this effect, because the grain then re-equilibrates along the adsorption branch of its isotherm, whose equilibrium moisture content is lower for the same water activity [37, 38]. Ethnographic work likewise attributes the durability of stored paddy to the building together with customary rules of planting, harvesting and storage [23]. Hygrothermal damping is thus one component of a multi-causal preservation system; grain quality and spoilage were not measured.

3.6 Site dependence: Leuit 3 as a case study

L3 does not follow the pattern of L1 and L2. Its exterior series shows a clear diurnal cycle ($R^2 = 0.668$ for T and 0.787 for RH), but its interior series is essentially flat (amplitudes of 0.29 °C and 0.47%, SNR below 0.7; $R^2 = 0.174$ and 0.110). The interior signal is a slow, almost linear drift rather than a diurnal wave: over 144 h, temperature fell by 1.16 °C and RH rose by 3.28 percentage points, with residual SDs after detrending of only 0.37 °C and 0.30 percentage points, and its RH amplitude has the opposite sign to every other series. L3 was therefore excluded from Tables 2 and 3.

In the field, this behaviour is attributed to site factors rather than construction: L3 stands beneath a very dense forest

canopy, and its owner reportedly packed the bundles more tightly. The gridded product cannot represent metre-scale shading, so its exterior amplitude of 2.77 °C does not measure the forcing that reached the L3 walls. However, the exterior daily means at L3 differ from those at L1 by amounts that reverse sign between cycles (+1.50 to −0.86 °C; −6.4 to +8.6 percentage points), which cannot originate in spatial differences within one grid cell. Specimen differences are therefore confounded with weather, and the canopy explanation remains plausible rather than demonstrated. L3 is therefore treated as a case study rather than as a control: because the forcing at its walls is unknown, it shows only that a flat interior record cannot by itself demonstrate system performance, since it can equally arise from weak local forcing.

3.7 Moisture buffering and design translation for low-energy storage

Hygroscopic buffering capacity is conventionally quantified by the Moisture Buffer Value (MBV), measured gravimetrically under cyclic humidity steps on samples of known surface area and expressed in g m^{-2} $\%RH^{-1}$ [19, 43, 44]. Without gravimetric data, no standard-compliant MBV can be computed here. The RH amplitude ratio ($f = 0.22 \pm 0.02$), together with the phase relations in Table 4, is therefore reported only as an indirect, system-level indicator consistent with sorption-based buffering. The two are not interchangeable: f describes an assembled system under a specific forcing and geometry, whereas MBV is a material property. Determining MBV on the Leuit materials under the NORDTEST protocol will require new sampling.

Conventional facilities counter storage fluctuations with thermal drying and mechanical ventilation [1, 2, 45], and the present results add a field data point to the literature on coupled heat and moisture transfer in bio-based porous media [46-49] and on the buffering capacity of plant-biomass walls [19]. The Leuit operates without operational energy, but a quantitative avoided-emission estimate would require a defined counterfactual store, measured grain mass and storage duration, none of which this study provides. The design value of the findings is therefore expressed through performance indicators rather than carbon figures.

Table 6 translates the measured indicators into provisional design benchmarks. They are conditional on the reanalysis forcing and on two specimens monitored in different weather windows, so they describe what a Leuit-type store achieved under these conditions rather than general targets. Each indicator is linked to the envelope and storage features expected to control it and to the measurement needed to verify it. Figure 5 organises the same indicators into a measurement-to-design framework for low-energy stores in the humid tropics: exterior, inner-wall and in-stack sensors are deployed simultaneously; harmonic parameters, Λ_T, the phase of e_{in} relative to T_{in} and e_{out}, and the baseline RH are computed; and the diagnosis guides material and geometry choices, followed by re-measurement. Where the vapour channel is sorption-dominated, envelope and storage materials should be selected for sorption capacity and exposed hygroscopic surface rather than for thermal mass alone. The Leuit thus illustrates how a design that evolved in dialogue with its natural setting can inform low-energy, nature-based storage infrastructure [4].

Table 6. Design translation of the measured indicators (L1 and L2; provisional and conditional on the reanalysis forcing)

Indicator	Measured (L1; L2)	Provisional Benchmark	Envelope and Storage Features Expected to Control it	Verification in Practice
f_T	0.61; 0.70	≤0.70 under comparable forcing	Envelope thickness and diffusivity, roof shading, raised floor, thermal capacity of the stack	Shaded exterior logger and in-stack logger; Eqs. (2) and (3)
$\Delta\varphi_T$ (h)	1.39; 1.33	≥1.3 h	As for f_T	Crest times of the paired fits; Eq. (4)
Λ_T	1.36 ± 0.31; 1.03 ± 0.25	≈1 (diagnostic, not a target)	Λ < 1: advective short-circuit through openings; Λ > 1: additional storage	Eq. (8) with forcing measured at the wall
f_{RH}	0.23; 0.20	≤0.25 (descriptive)	Exposed hygroscopic surface (panicle bundles, bamboo, palm fibre), vapour-open envelope, limited openings	Same loggers; check exterior saturation
Crest of $e_{in} - T_{in}$ (h)	−0.55; −0.78	|difference| < 1 h: sorption-dominated vapour channel	Hygroscopic stored mass, low air exchange	e from logger T and RH (Magnus)
Amplitude ratio of e (in/out)	2.99; 2.73	>1: internal vapour source	Sorption capacity of stored mass and envelope	Exterior e from a ground logger
Baseline RH_{in} (%)	84.5; 86.1	Below equilibrium RH of paddy at ≤14% w.b. [28, 37, 38]	Pre-drying, site drainage, canopy exposure, raised floor	Daily mean of the in-stack record

3.8 Limitations

Five limitations bound these findings. First, the results derive from two specimens, each monitored once in non-overlapping windows across the dry-to-wet transition, so specimen differences are confounded with weather and dry-season extremes are not captured. Second, exterior data come from one reanalysis grid cell without a ground reference; f, $\Delta\varphi$ and Λ are therefore relative to a coarse proxy, and Λ_T is sensitive to plausible forcing errors (Section 3.3); calibrated loggers at the wall surface are the highest priority, particularly for the vapour channel. Third, nocturnal RH saturation and the semi-infinite assumption make the absolute f and Λ for RH indicative, and the residual-based SEs, which ignore serial correlation, are lower bounds. Fourth, sensor placement inside the stack prevents separating envelope and stored-mass contributions, and advection, bilik diffusivity, sugar-palm fibre properties and logger offsets were not determined. Fifth, without gravimetric or grain-quality data, f_{RH} is not an MBV and the preservation link is a plausible mechanism rather than a demonstrated outcome.

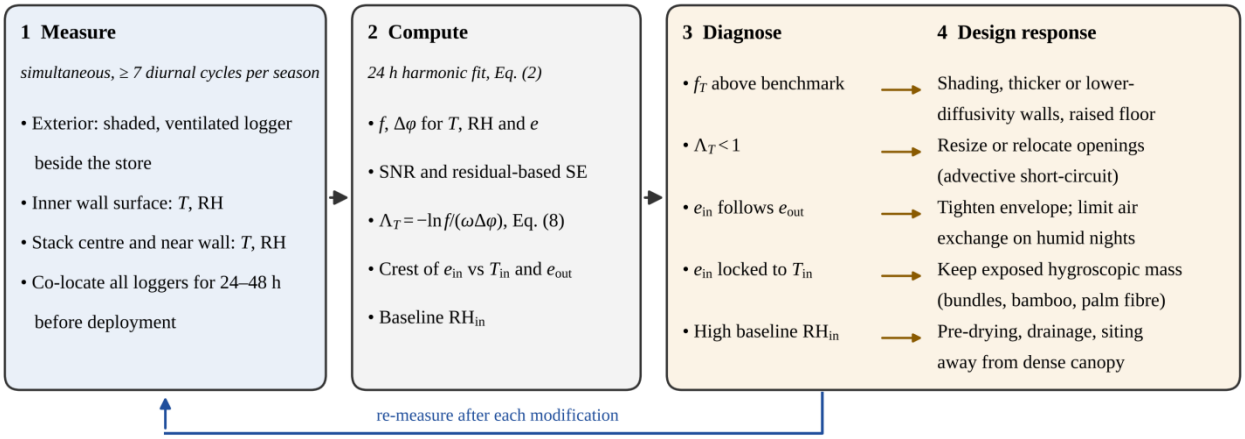

Figure 5. Measurement-to-design framework for low-energy bio-based stores in the humid tropics

4. CONCLUSIONS

This study provides an in-situ harmonic characterisation of the diurnal temperature and humidity response at the centre of the paddy stack in the vernacular Leuit Baduy rice granary, together with a diagnostic check of whether passive diffusion is consistent with it. At the two specimens with measurable exterior excitation, and relative to reanalysis forcing, the system damped the temperature amplitude to about 65% of its exterior value (f = 0.65 ± 0.06, mean ± SD, n = 2) with a lag of 1.36 ± 0.04 h, and the RH amplitude to about 22% (f = 0.22 ± 0.02) with a lag of 2.58 ± 0.59 h. The diagnostic ratio placed the heat channel within about one SE of Fourier diffusion (Λ = 1.36 ± 0.31 and 1.03 ± 0.25), which is consistent with, but not proof of, conductive transmission given the uncertainty of the forcing.

The strongest result concerns the vapour channel at the logged point: in-stack vapour pressure was locked in phase with in-stack temperature (crest difference below 0.8 h) and offset by about nine hours from exterior vapour pressure, and its amplitude was about three times the reanalysis amplitude. This pattern indicates that temperature-driven sorption and desorption in the paddy bundles and the envelope generate the in-stack humidity cycle locally, rather than the transmission of an exterior humidity wave. The canopy-shaded third specimen, whose forcing is unknown, is a case study showing that a flat interior record alone does not demonstrate performance.

For design, the results identify sorption capacity and exposed hygroscopic surface, rather than thermal mass alone, as the levers for passive humidity control in bio-based storage, and the study converts them into provisional indicators and a measurement framework. Given that the results rest on two specimens and reanalysis forcing, they constitute a preliminary quantitative baseline rather than a generalised model of Baduy vernacular architecture. Future work should monitor several specimens simultaneously with on-site exterior and inner-wall sensors, extend monitoring across seasons and determine MBV and grain-quality outcomes on the same structures.

ACKNOWLEDGMENT

The authors thank the customary head and the Baduy community of Kanekes Village for their permission and guidance. This work is supported by the Institute for Research and Community Service (LPPM), Universitas Sultan Ageng Tirtayasa, through an Internal Basic Research Grant (PDI) (Contract number: B/650.8/UN.43.9/PT.01.03/2026). The funder had no role in the study design, data collection and analysis, or manuscript preparation. The raw and hourly time series, the NASA POWER input files and the analysis scripts are provided as Supplementary Material, as described in Section 2.6.

DECLARATION OF AI USE

The authors used an AI assistant (Claude, Anthropic) for language editing, structural reorganisation and literature searching. The research design, fieldwork, data collection, analysis and scientific decisions are the authors' own; the authors verified all outputs, including numerical results and references, and take full responsibility for the content.

REFERENCES

[1] Ziegler, V., Paraginski, R.T., Ferreira, C.D. (2021). Grain storage systems and effects of moisture, temperature and time on grain quality—A review. Journal of Stored Products Research, 91: 101770. https://doi.org/10.1016/j.jspr.2021.101770

[2] Duangkhamchan, W., Huangsaeng, K., Kondo, N., Jaisut, D. (2024). Enhancing paddy rice preservation in small-scale barns: Comparative analysis of hot air-drying techniques and ventilation impact on quality and energy efficiency. Foods, 13(5): 672. https://doi.org/10.3390/foods13050672

[3] He, M., Li, L., Tao, S. (2024). Sustainable design methods translated from the thermodynamic theory of vernacular architecture: Atrium prototypes. Buildings, 14(10): 3142. https://doi.org/10.3390/buildings14103142

[4] Nursaniah, C., Qadri, L., Fuady, Z. (2025). Relearning vernacular wisdom for thermal comfort: Assessing climate-responsiveness in modern housing clusters of Banda Aceh. International Journal of Design & Nature and Ecodynamics, 20(9): 2109-2119.

https://doi.org/10.18280/ijdne.200915
[5] Peng, Y., Zhang, X.Y., Li, X.F. (2023). Effect of phase lags of moisture–heat flow on the hygrothermoelastic field of hollow cylinders with convective surfaces. Mechanics Based Design of Structures and Machines, 51(6): 3004-3025. https://doi.org/10.1080/15397734.2021.1914654
[6] Zhou, X., Desmarais, G., Carl, S., Mannes, D., Derome, D., Carmeliet, J. (2022). Investigation of coupled vapor and heat transport in hygroscopic material during adsorption and desorption. Building and Environment, 214: 108845. https://doi.org/10.1016/j.buildenv.2022.108845
[7] Aliyari, N., Fernandes, M.S., Gaspar, A.R. (2026). Solid-gas thermochemical energy storage systems: A critical review. Journal of Energy Storage, 155: 121166. https://doi.org/10.1016/j.est.2026.121166
[8] Daunais, N., Zou, Y., Coussot, P. (2026). A physical approach to the modeling of hygrothermal transfers in bio-based construction and textile materials. International Journal of Heat and Mass Transfer, 256(Part 1): 127973. https://doi.org/10.1016/j.ijheatmasstransfer.2025.127973
[9] Mmari, W., Johannesson, B. (2022). A model for multiphase moisture and heat transport below and above the saturation point of deformable and swelling wood fibers—I: Mass transport. Applications in Engineering Science, 12: 100117. https://doi.org/10.1016/j.apples.2022.100117
[10] Qi, P.X., Xu, J.J., Li, H.Y., Luo, J.P., Shi, Q. (2025). Sorption mechanism, hygroscopic agents, and application of passive water evaporative cooling technology—A review. Chemical Thermodynamics and Thermal Analysis, 18: 100166. https://doi.org/10.1016/j.ctta.2025.100166
[11] Asan, H. (2006). Numerical computation of time lags and decrement factors for different building materials. Building and Environment, 41(5): 615-620. https://doi.org/10.1016/j.buildenv.2005.02.020
[12] Moolavi Sanzighi, S., Soflaei, F., Shokouhian, M. (2021). A comparative study of thermal performance in three generations of Iranian residential buildings: Case studies in CSA Gorgan. Journal of Building Physics, 44(4): 326-363. https://doi.org/10.1177/1744259120906241
[13] Dolker, T., Katiyar, A.K., Chaurasia, O.P., Stobdan, T. (2025). Vegetable storage in freezing winter: A survey in trans-Himalayan Ladakh, India. Journal of Food and Agriculture Research, 5(1): 27-35. https://doi.org/10.47509/JFAR.2025.v05i01.03
[14] Toure, P.M., Dieye, Y., Gueye, P.M., Sambou, V., Bodian, S., Tiguampo, S. (2019). Experimental determination of time lag and decrement factor. Case Studies in Construction Materials, 11: e00298. https://doi.org/10.1016/j.cscm.2019.e00298
[15] Pérez-García, O.A., Carreira, X.C., Carral, E., Fernández, M.E., Mariño, R.A. (2010). Evaluation of traditional grain store buildings (hórreos) in Galicia (NW Spain): Analysis of outdoor/indoor temperature and humidity relationships. Spanish Journal of Agricultural Research, 8(4): 925-935. https://doi.org/10.5424/sjar/2010084-1210
[16] Klemczak, B., Smolana, A., Jędrzejewska, A. (2024). Modeling of heat and mass transfer in cement-based materials during cement hydration—A review. Energies, 17(11): 2513. https://doi.org/10.3390/en17112513
[17] Benzaama, M.H., Braga-Neto, U. (2026). Hybrid AI and physics modelling approaches for hygrothermal behavior of bio-based building materials: Challenges, limitations and perspectives. Energy and Buildings, 360: 117327. https://doi.org/10.1016/j.enbuild.2026.117327
[18] Caruso, L., Buhagiar, V., Caruana Smith, G., Larcher, M., Buhagiar, S., Bottino Leone, D. (2025). Hygrothermal performance of an innovative resource efficient composite masonry unit with embedded biobased insulation. Energy and Buildings, 344: 116015. https://doi.org/10.1016/j.enbuild.2025.116015
[19] Ndukwu, M.C., Simo-Tagne, M., Ekop, I.E., et al. (2023). Energy in buildings: A review of models on hygrothermal transfer through the porous materials for building envelope. Future Technology, 2(4): 33-44. https://doi.org/10.55670/fpll.futech.2.4.4
[20] Maaroufi, M., Bennai, F., Belarbi, R., Abahri, K. (2021). Experimental and numerical highlighting of water vapor sorption hysteresis in the coupled heat and moisture transfers. Journal of Building Engineering, 40: 102321. https://doi.org/10.1016/j.jobe.2021.102321
[21] Nugroho, A.M., Kubota, T., Alfata, M.N.F., Putri, F.A., Iyati, W. (2026). Passive design strategies of vernacular houses in the hot-humid climate of Indonesia. VITRUVIO—International Journal of Architectural Technology and Sustainability, 11(1): e24735. https://doi.org/10.4995/vitruvio-ijats.2026.24735
[22] Angkasa, Z., Kamil, E.M. (2024). Passive cooling in Indonesian traditional dwellings and its relationship with geographical location. Journal of Design and Built Environment, 24(1): 1-16. https://doi.org/10.22452/jdbe.vol24no1.1
[23] Tresnasih, R.I., Lasmiyati, Rostiyati, A., Merlina, N. (2023). Leuit as a symbol of local wisdom [in Indonesian]. Paradigma: Jurnal Kajian Budaya, 13(2): 159-176. https://doi.org/10.17510/paradigma.v13i2.1269
[24] Farokhah, L., Supriatna, M., Herman, T., Abidin, Z., Zulfadhli, M. (2023). Ethnomathematics exploration on the Leuit Lenggang of the Baduy tribe in Banten Province Indonesia. AIP Conference Proceedings, 2727: 020052. https://doi.org/10.1063/5.0141668
[25] Yulia, R., Prakarsa, A., Fauzi, A. (2018). Leuit Baduy: A food security in Baduy customary law. Mimbar: Jurnal Sosial dan Pembangunan, 34(2): 265-273. https://doi.org/10.29313/mimbar.v34i2.3415
[26] Iskandar, J., Iskandar, B.S. (2017). Ecological wisdom of the Baduy people in paddy conservation through the "leuit system" [in Indonesian]. Jurnal Biodjati, 2(1): 38-51. https://doi.org/10.15575/biodjati.v2i1.1289
[27] Septiawan, B. (2008). Analysis of functional, structural design and microclimate conditions in the traditional rice barn (Leuit) of the Outer Baduy community in Banten province [in Indonesian]. Undergraduate thesis, Institut Pertanian Bogor, Bogor, Indonesia. http://repository.ipb.ac.id/handle/123456789/50105.
[28] Badan Standardisasi Nasional. (2023). SNI 224:2023 Gabah (Paddy) [in Indonesian]. Jakarta, Indonesia. https://akses-sni.bsn.go.id.
[29] Gelaro, R., McCarty, W., Suárez, M.J., et al. (2017). The modern-era retrospective analysis for research and

applications, version 2 (MERRA-2). Journal of Climate, 30(14): 5419-5454. https://doi.org/10.1175/JCLI-D-16-0758.1
[30] Zhang, X., Li, J., Yu, Y., Wang, H. (2018). Investigating the water vapor sorption behavior of bamboo with two sorption models. Journal of Materials Science, 53(11): 8241-8249. https://doi.org/10.1007/s10853-018-2166-y
[31] Chen, Q., Wang, G., Ma, X.X., Chen, M.L., Fang, C.H., Fei, B.H. (2020). The effect of graded fibrous structure of bamboo (Phyllostachys edulis) on its water vapor sorption isotherms. Industrial Crops and Products, 151: 112467. https://doi.org/10.1016/j.indcrop.2020.112467
[32] Nguyen, D.M., Grillet, A.C., Diep, T.M.H., Ha Thuc, C.N., Woloszyn, M. (2017). Hygrothermal properties of bio-insulation building materials based on bamboo fibers and bio-glues. Construction and Building Materials, 155: 852-866. https://doi.org/10.1016/j.conbuildmat.2017.08.075
[33] Ishak, M.R., Sapuan, S.M., Leman, Z., Rahman, M.Z.A., Anwar, U.M.K., Siregar, J.P. (2013). Sugar palm (Arenga pinnata): Its fibres, polymers and composites. Carbohydrate Polymers, 91(2): 699-710. https://doi.org/10.1016/j.carbpol.2012.07.073
[34] Yuan, J., Chen, Q., Fang, C., Zhang, S., Liu, X., Fei, B. (2021). Effect of chemical composition of bamboo fibers on water sorption. Cellulose, 28(11): 7273-7282. https://doi.org/10.1007/s10570-021-03988-3
[35] Yin, X., Lawrence, M., Maskell, D., Ansell, M. (2018). Comparative micro-structure and sorption isotherms of rice straw and wheat straw. Energy and Buildings, 173: 11-18. https://doi.org/10.1016/j.enbuild.2018.04.033
[36] El Moussi, Y., Clerc, L., Bénézet, J.C. (2023). Design of a novel hybrid rice straw/husk bio-based concrete featuring enhanced mechanical and hygrothermal properties. Waste and Biomass Valorization, 14(1): 345-363. https://doi.org/10.1007/s12649-022-01854-2
[37] Zeymer, J.S., Corrêa, P.C., Oliveira, G.H.H., Baptestini, F.M., Campos, R.C. (2019). Mathematical modeling and hysteresis of sorption isotherms for paddy rice grains. Engenharia Agrícola, 39(4): 524-532. https://doi.org/10.1590/1809-4430-eng.agric.v39n4p524-532/2019
[38] Mousa, W., Ghazali, F.M., Jinap, S., Ghazali, H.M., Radu, S. (2014). Sorption isotherms and isosteric heats of sorption of Malaysian paddy. Journal of Food Science and Technology, 51(10): 2656-2663. https://doi.org/10.1007/s13197-012-0799-4
[39] Perré, P., Ferreira da Silva, Y., Mazian, B., Augusto, P.E.D., Rémond, R. (2026). Low-cost hygroscopic packed beds for energy storage in solar dryers: Sizing rules from a dual-scale heat and mass transfer model. Journal of Energy Storage, 153: 121069. https://doi.org/10.1016/j.est.2026.121069
[40] Palumbo, M., Lacasta, A.M., Giraldo, M.P., Haurie, L., Correal, E. (2018). Bio-based insulation materials and their hygrothermal performance in a building envelope system (ETICS). Energy and Buildings, 174: 147-155. https://doi.org/10.1016/j.enbuild.2018.06.042
[41] Ouma, F., Luthra, K., Oduola, A., Atungulu, G.G. (2024). Investigating safe storage conditions to mitigate aflatoxin contamination in rice. Food Control, 163: 110529. https://doi.org/10.1016/j.foodcont.2024.110529
[42] Paderes, D.E. (1997). Influence of moisture content and length of storage on fungal invasion of paddy rice. BIOTROPIA, 10: 1-13. https://doi.org/10.11598/btb.1997.0.10.129
[43] Cascione, V., Maskell, D., Shea, A., Walker, P. (2021). The moisture buffering performance of plasters when exposed to simultaneous sinusoidal temperature and RH variations. Journal of Building Engineering, 34: 101890. https://doi.org/10.1016/j.jobe.2020.101890
[44] Zu, K., Qin, M., Rode, C., Libralato, M. (2020). Development of a moisture buffer value model (MBM) for indoor moisture prediction. Applied Thermal Engineering, 171: 115096. https://doi.org/10.1016/j.applthermaleng.2020.115096
[45] Yin, Q., He, Y., Liu, S., et al. (2025). Heat and moisture transfer dynamics in humidity-stratified paddy grain bulk under mechanical ventilation. Results in Engineering, 27: 106131. https://doi.org/10.1016/j.rineng.2025.106131
[46] Kulish, V., Phan, B.T., Horák, V. (2025). A non-field analytical solution of the Luikov equations for simultaneous heat and mass transfer. Results in Engineering, 25: 104534. https://doi.org/10.1016/j.rineng.2025.104534
[47] Ravshanov, N., Shadmanov, I., Kubyashev, K., Khikmatullaev, S. (2021). Mathematical modeling and research of heat and moisture transfer processes in porous media. E3S Web of Conferences, 264: 01038. https://doi.org/10.1051/e3sconf/202126401038
[48] Koukouch, A., Bakhattar, I., Asbik, M., Idlimam, A., Zeghmati, B., Aharoune, A. (2020). Analytical solution of coupled heat and mass transfer equations during convective drying of biomass: Experimental validation. Heat and Mass Transfer, 56: 1971-1983. https://doi.org/10.1007/s00231-020-02817-w
[49] Wassel, M., Mousa, M., Fouda, A., Jehad, M. (2013). Theoretical study of affecting parameters on drying process of organic materials. Mansoura Engineering Journal, 38(3): 24-39. https://doi.org/10.21608/bfemu.2020.106986

NOMENCLATURE

A	amplitude of the harmonic model, °C, % or hPa
D_{eff}	effective vapour diffusivity, $m^2\ s^{-1}$
e	water-vapour pressure, hPa
e_s	saturation vapour pressure, hPa
f	amplitude ratio, dimensionless
k	amplitude scaling factor of the exterior forcing, dimensionless
L	effective path length, m
n	number of hourly values in a series, dimensionless
P_V	water-vapour pressure in Eq. (5b), Pa
R^2	coefficient of determination, dimensionless
RH	relative humidity, %
s	residual standard deviation, °C, % or hPa
SNR	signal-to-noise ratio $\|A\|/s$, dimensionless
T	temperature, °C
t	time, h
U	measurement uncertainty, °C or %
W	half period of the harmonic model, h
x	depth coordinate, m
x_c	phase shift of the harmonic model, h
y, y_0	measured variable, baseline mean, °C or %

Greek symbols

α	thermal diffusivity, $m^2\ s^{-1}$
δ	phase shift applied to the exterior forcing, h
$\Delta\varphi$	time lag, h
Λ	diagnostic ratio, Eq. (8), dimensionless
ω	diurnal angular frequency, $\pi/12$ rad h^{-1}

Subscripts

external	satellite (reanalysis) term
in	interior (in-stack logged point)
internal	logger term
out	exterior
RH	relative humidity channel
T	temperature channel
total	combined

APPENDIX

A1. Residual-based SE. For a 24 h harmonic fitted by least squares to n evenly spaced hourly values spanning whole cycles, the sine and cosine regressors are orthogonal, the model sum of squares equals $nA^2/2$, and the two coefficient errors are uncorrelated with equal variance $2s^2/n$. Hence $s = [nA^2(1 - R^2)/(2R^2(n - 4))]^{1/2}$, $\mathrm{SE}(A) = s(2/n)^{1/2}$ and $\mathrm{SE}(x_c) = (12/\pi)\mathrm{SE}(A)/|A|$ in hours. Because constant weights leave least-squares estimates unchanged, A, x_c and R^2 do not depend on the weighting; only the SEs do. Errors were propagated as $\mathrm{SE}(f) = f[(\mathrm{SE}(A_{in})/A_{in})^2 + (\mathrm{SE}(A_{out})/A_{out})^2]^{1/2}$, $\mathrm{SE}(\Delta\varphi) = [\mathrm{SE}(x_{c,in})^2 + \mathrm{SE}(x_{c,out})^2]^{1/2}$, $\mathrm{SE}(-\ln f) = \mathrm{SE}(f)/f$ and $\mathrm{SE}(\Lambda) = \Lambda[(\mathrm{SE}(-\ln f)/(-\ln f))^2 + (\mathrm{SE}(\Delta\varphi)/\Delta\varphi)^2]^{1/2}$, amplitude and phase errors being uncorrelated for whole cycles.

A2. Upper bound on the SE of the interior *e* phase. Linearising the Magnus relation about the series mean expresses a small departure of e as $(e_s/100)$ times that of RH plus $(\mathrm{RH}/100)(de_s/dT)$ times that of T, where e_s is the saturation vapour pressure. Because the fitted e harmonic minimises the residual sum of squares, its residual standard deviation (SD) cannot exceed that of the same combination of the T and RH harmonics, which by the triangle inequality is at most $(e_s/100)s_{RH} + (\mathrm{RH}/100)(de_s/dT)s_T$. With the Table 1 values, this bound is 2.5 hPa at both specimens, giving $\mathrm{SE}(x_c) \le 0.62$ h (L1) and ≤ 0.40 h (L2) for interior e (Table 4).

A3. Sensitivity of Λ to forcing error. If the local exterior amplitude equals k times the reanalysis amplitude and the local exterior crest occurs δ hours earlier than the reanalysis crest, $\Lambda = (-\ln f + \ln k)/[\omega(\Delta\varphi + \delta)]$. Table A1 gives the values k^* and δ^* at which $\Lambda = 1$, each with the other parameter at its nominal value, and the range of Λ for $k = 0.8$ to 1.2.

Table A1. Sensitivity of the diagnostic ratio to errors in the exterior forcing

Specimen	Variable	Λ	k^*	δ^* (h)	Λ (k = 0.8–1.2)
L1	T	1.36	0.88	0.50	0.75–1.86
L2	T	1.03	0.99	0.03	0.38–1.55
L1	RH	2.57	0.41	3.38	2.17–2.89
L2	RH	2.03	0.44	3.10	1.75–2.26